On the Relationship between the Chromium Concentration, the Z-Phase Formation and the Creep Strength of Ferritic-Martensitic Steels

Yu, Hao; Xu, Wei; van der Zwaag, Sybrand

DOI
10.1002/srin.201800177

Publication date
2018

Document Version
Final published version

Published in
Steel Research International

steel research international
www.steel-research.de

On the Relationship between the Chromium Concentration, the *Z*-Phase Formation and the Creep Strength of Ferritic-Martensitic Steels

Hao Yu, Wei Xu, and Sybrand van der Zwaag*

In this study, the long term creep strength behavior of commercial heat resistant martensitic/ferritic steels with Cr levels ranging from 1 to 15 wt% is analyzed by linking their computed equilibrium compositions to their creep properties. At lower Cr levels, the calculated strength due to precipitation hardening agrees well with the experimental results. At high chromium levels and longer exposure times, an accelerated strength loss due to the formation of Z-phase precipitates has been reported. The accelerated strength loss is computationally analyzed and a correlation between accelerated strength loss and Z-phase formation is confirmed. A study is made to explore the option of adjusting the chemical composition of existing high-chromium steels to reduce the driving force for Z-phase formation. However, no proper composition ranges are found which combine a high Cr concentration with a significantly lower driving force for Z-phase formation.

1. Introduction

Creep resistant steels that combine a high creep strength with a high corrosion and oxidation resistance are a key requirement for the construction of efficient and long-lasting power plants. Power plant design has sought to increase the overall fuel efficiency by bringing the operating conditions to higher pressures and temperatures. The increase in the severity of the operating conditions has led to ongoing research into the development of creep-resistant steels with even more outstanding mechanical properties and corrosion resistance at elevated temperatures.[1] The development has also led to a renewed interest in understanding the role of chromium concentration in the time dependent creep strength.

Low-alloy ferritic/bainitic steels with low chromium and molybdenum levels (1/2Cr1/2Mo, 1CrMo, 2CrMo etc.), which were developed at the beginning of the 1920s, were commonly used for the components of the first generation power station boilers. It was general practice to use these steels for installations with a service temperature between 450 and 500 °C and a pressure of 35 bar.[2] However the increase in service temperature and service pressure has necessitated the raise of the chromium level in such steels. Progress in recent years has led to the development of high-strength 9–12% Chromium martensitic steels.[3,4] Their high creep strength at 600 °C is guaranteed by the tempered martensitic matrix, containing solid solution strengthening alloying elements and particle strengthening with carbonitrides.[5–7] With higher operating temperatures approaching 650 °C, even higher Cr levels are required for better oxidation resistance. To ensure a fully martensitic microstructure, the increased chromium content has to be balanced by the addition of elements that stabilize the austenite phase without reducing the ferrite/austenite transformation temperature. Cobalt and copper have been the favored additions and the newer 12% chromium steels usually contain one of these elements. However, attempts to apply 12% Cr steels at 650 °C have largely failed, since under this condition the fine MX particles which provide a major strengthening contribution transform into relatively coarse *Z*-phase particles.[8–10] The development of *Z*-phase has been held responsible for the decrease in long term creep properties as well as the decrease in corrosion resistance, since the formation of *Z*-phase not only causes the dissolution of desirable MX precipitates,[11] but it also might consume some of the chromium in solid solution in the matrix which is required for the formation of a corrosion resistant surface layer. In Hald's research,[10] one possible solution to avoid *Z*-phase in high Cr steels is to eliminate the *Z*-phase forming elements such as V and Nb and replace them by Ti, since TiN is the only nitride in steels which cannot transform into *Z*-phase. However, the TiN nitrides generally do not make a significant contribute to the high temperature strength, hence, the problem how to suppressing *Z*-phase formation in heat resistant martensitic steels with high Cr levels (Cr wt% > 11) operating under a prescribed service temperature of 600–650 °C still remains unsolved.[12]

Prof. W. Xu
State Key Laboratory of Rolling and Automation
Northeastern University
110819 Shenyang, P. R. China
E-mail: W.Xu@tudelft.nl

Prof. W. Xu, H. Yu, Prof. S. van der Zwaag
Novel Aerospace Materials group
Faculty of Aerospace Engineering
Delft University of Technology
2629HS Delft, The Netherlands

The ORCID identification number(s) for the author(s) of this article can be found under https://doi.org/10.1002/srin.201800177.

DOI: 10.1002/srin.201800177

The development of creep resistant steels functioning at higher temperatures required a new concept for high chromium steel,[13] and led to the development of fully ferritic steels with a chromium content of 14% or more, not undergoing a martensitic transformation. Due to the extremely low solubility of carbon and nitrogen in ferrite, it will not be possible to produce a significant and stable dispersion of strengthening carbides and nitrides. Instead, intermetallic phases, such as the Laves phases, should be considered provided that such precipitates are sufficiently fine and resistant to coarsening at the applied temperatures. To validate the feasibility of a ferritic matrix, Kimura et al.[14] have investigated the effect of initial microstructure on the long-term creep strength, assuming that fully annealed steels with a ferritic matrix and a relatively low dislocation density would perform better under long-term service conditions. Based on this concept, novel ferritic steels with 15% Cr level have been developed in which the precipitation strengthening is due to intermetallic compounds.[15] However, as stated above the formation of strengthening intermetallic particles consumes Cr in solid solution. Also, a high level of Cr leads to a microstructural instability and strongly promotes the formation of a detrimental *Z*-phase during long time creep exposure. Whether the remaining Cr content in the matrix can ensure the long term oxidation resistance at elevated service temperature appears doubtful.[16] As on the one hand a sufficiently high Cr level is beneficial for high temperature corrosion and oxidation stability, while on the other hand an increase in Cr level promotes the formation of a detrimental phase, it is useful to analyze the possibility to tailor the overall chemical composition of high Cr ferritic steels to reduce the tendency to *Z*-phase formation.

The present study is a thermodynamic/computational analysis of both the creep strength behavior as a function of the Cr level over the range 1–15 wt% and an exploration of compositional modifications to reduce *Z*-phase formation in 15 wt% Cr steels to be used at 650 °C or above.

2. Results and Discussion

2.1. Existing Martensitic/Ferritic Steel with Different Cr Level

Table 1 shows the chemical composition of some existing heat resistant steels listed in order of their Cr level,[2,15,17–19] and decade in which the steel was introduced in the market is reported.[1,2] For the commercial grades, the specification ranges of their alloying elements are listed as well. As mentioned above, these heat resistant steels can be roughly divided into three groups: Low-alloy ferritic steels (1–4%Cr); 9–12Cr martensitic steels and 15Cr ferritic steels. The chemical compositions of the low-alloy ferritic steels are quite similar in their C, Si, Mn, and Mo levels, yet have different Cr levels. Si is a ferrite former whereas Mn is an austenite former. The Mn/Si balance controls the high temperature stability of the ferritic matrix and also contributes to a proper toughness. The addition of Mo provides some solid solution strengthening, thereby effectively enhancing the creep properties.[20]

With respect to 9–12Cr steels, the 15Cr steels are more heavily alloyed to achieve better high-temperature mechanical properties. All high Cr alloys contain a similar alloying level of V, Nb, and N, which produces finely distributed MX carbonitrides and a remarkable precipitation strengthening. In contrast, the alloying levels of Mo and W vary with the different steel grades. These elements not only act as solid solution strengtheners but also as Laves phase formers, in order to provide particle strengthening. The addition of austenite stabilizers such as Co, Ni, and Cu, to high-Cr grades (Cr% > 11%), aims to maintain the Cr equivalent while inhibiting the formation of δ-ferrite The Boron addition, according to the literature,[21,22] helps to retard the coarsening of the $M_{23}C_6$ carbides near the prior austenite grain boundaries, which decreases the minimum creep rate and increases the time to rupture. As shown in Table 1, the 15Cr ferritic steels are relatively highly alloyed with Mo, W, and Co compared to 9–12Cr grades, the effect of which on the mechanical properties will be discussed in the next section.

The equilibrium phase fractions of the various strengthening phases (in vol%) at a service temperature of 650 °C, as calculated by Thermo-Calc are listed in **Table 2**. Here, the thermodynamic calculation ignores the effects of applied stresses on their equilibrium phase configuration, since the simulation of stress field is beyond the ability of Thermo-Calc calculation. For low-alloy steels with a ferritic matrix, only $M_{23}C_6$ carbides play a significant role as strengthening particles, and the amount of $M_{23}C_6$ particles increases slightly with the addition of Cr. Despite the difference in chemical concentration, the 9–12%Cr steel grades share an almost identical as-tempered martensitic matrix. The characteristics of the precipitates present, such as the $M_{23}C_6$ or the Laves phase, intrinsically determine the creep properties during service, as the precipitates pin the movement of dislocations, that is, reduce the creep rate, and retard the recovery of martensitic lath boundaries. Compared to low-alloy steels, the higher amount of precipitates in 9–12%Cr steels provides a considerable contribution to the high-temperature properties. According to the thermodynamic calculations the undesirable coarse *Z*-phase particles can be present in 9–12Cr and 15Cr steels, while no MN phases are identified. The reason is that MN nitrides are thermodynamically less stable than the *Z*-phase according to Danielsen's research.[8,23] The precipitation of *Z*-phase at the expense of MN nitrides has been confirmed as the root cause of the observed premature failure during long-time creep test. 15Cr steels contain a higher amount of Laves phase particles which act as their major strength contributor.

2.2. Creep Properties of Existing Martensitic/Ferritic Steel

Figure 1 shows the reported creep strength values of existing Cr-containing steels as a function of time at a fixed temperature of 650 °C.[2,6,15,17,24] As intended, the low-alloying heat resistance steels show a much lower creep rupture stress compared to high Cr containing steels for a given rupture time, since low alloying steels are designed to operate at the temperature below 500 °C. Within the low-alloyed steel group, only minor differences in creep properties can be found. The complex dependence of creep properties on alloying conditions and service condition can hardly be analyzed systematically, and the effect of Cr content on

Table 1. Chemical composition of existing Cr steels grades (in wt%, with Fe to balance), and year of conception when the steel was introduced in the market.

	C	Si	Mn	Cr	Mo	W	V	Nb	B	N	others	Year of conception
P11/ STBA22[17]	0<⁄0.15⁄≤0.15	0.50<⁄0.65⁄<1.00	0.30<⁄0.50⁄<0.60	0.90<⁄1.00⁄<1.10	0.45<⁄0.50⁄<0.65							1920s
STBA23[17]	0<⁄0.15⁄≤0.15	0.50<⁄0.65⁄<1.00	0.30<⁄0.45⁄<0.60	1.00<⁄1.25⁄<1.50	0.45<⁄0.50⁄<0.65							1920s
P22/ STBA24[17]	0<⁄0.15⁄≤0.15	0<⁄0.50⁄≤0.50	0.30<⁄0.45⁄<0.60	1.90<⁄2.25⁄<2.60	0.87<⁄1.00⁄<1.18							1930s
STBA25[17]	0<⁄0.15⁄≤0.15	0<⁄0.50⁄≤0.50	0.30<⁄0.45⁄<0.60	4.80<⁄5.00⁄<5.20	0.45<⁄0.50⁄<0.65							1930s
P9/STBA26[17]	0<⁄0.15⁄≤0.15	0<⁄0.50⁄≤0.50	0.30<⁄0.45⁄<0.60	8.00<⁄9.00⁄<10.00	0.90<⁄1.00⁄<1.10							1940s
P91[1]	0.08<⁄0,10⁄<0.12	0<⁄0,40⁄≤0.50	0.30<⁄0,45⁄<0.60	8.00<⁄9.00⁄<9.50	0.85<⁄1.00⁄<1.05		0.18<⁄0.20⁄<0.25	0.06<⁄0,08⁄<0.10		0.03<⁄0,05⁄<0.07		1970s
P92[1]	0.07<⁄0,10⁄<0.13	0<⁄0.50⁄≤0.50	0.30<⁄0,45⁄<0.60	8.50<⁄9.00⁄<9.50	0.30<⁄0.50⁄<0.60	1.50<⁄1,80⁄<2.00	0.15<⁄0.20⁄<0.25	0.04<⁄0,08⁄<0.09	0.001<⁄0,00⁄<0.006	0.03<⁄0,05⁄<0.07		1980s
MARN[18]	0,08	0,30	0,50	9		3.00	0.20	0.05		0.008	3.00Co	1990s
NF12[1]	0,10	0,20	0,50	10	0,15	2,60	0,20	0,06	0.004	0,07	2,50Co	1990s
SAVE12[19]	0,10	0,25	0,25	11		3.00	0,20	0,07	0.006	0,03	3.00Co, 0,10Ta,0.04Nd	1990s
P122[1]	0.07<⁄0,11⁄<0.14	0<⁄0,10⁄≤0.50	0<⁄0,60⁄≤0.70	10.00<⁄12.00⁄<12.50	0.25<⁄0.40⁄<0.60	1.50<⁄2.00⁄<2.50	0.15<⁄0.20⁄<0.30	0.04<⁄0,05⁄<0.10	0.0005<⁄0,003⁄<0.005	0.040<⁄0,06⁄<0.100	1.00Cu	1990s
15Cr3W3Co[15]	0,10	0,25	0,50	15	1.00	3.00	0,20	0,05	0,003	0,08	3.00Co	2000s
15Cr6W3Co[15]	0,05	0,22	0,50	15	1.00	6.00	0,19	0,045	0,003	0,033	3.00Co	2000s

The first value per element is the lowest specification range; the bold middle value is the value used in calculation; the final value is the highest specification range per element.

creep properties is largely submerged in the other influencing factors. The creep curves show that the 15Cr6W3Co, SAVE12, NF12, and P122 commercial and pre-commercial grades perform better than the other counterparts. A qualitative analysis by combining Figure 1 with the results in Tables I and II, the mentioned steels performing better generally contain higher levels of W + Mo, leading to higher amounts of Laves phases present. The contributions of the W, Mo-enriched Laves phase to the creep performances will be analyzed in the following section. Finally, a remarkable drop in creep strength at longer creep time can be found in 15Cr6W3Co, SAVE12, and P122 steels. The reason for the reduction in strength will be computationally analyzed.

As grain boundary strengthening does not play a major role in creep resistant steels, the precipitation hardening and solid solution strengthening are the most effective methods to raise the creep strength. In our previous work, the precipitation strengthening contribution in creep resistant steels has been shown to be inversely proportional to the inter-particle spacing, which in general is a function of the particle volume fraction, the initial particle size and coarsening kinetics of the precipitates.[25–27] The following expression is used to calculate the time-dependent precipitate strengthening factor while taking into account precipitate coarsening and its temperature dependence:

$$\sigma_p \propto {}^{1}\!/_{L} = \sqrt{f_p}\,/_{r} = \sqrt{f_p}\,/_{\sqrt[3]{r_0^3+Kt}} \tag{1}$$

$$\gamma_0 = {}^{2\gamma}\!/_{\Delta G_V} \tag{2}$$

$$K = {}^{8\gamma V_m^p}\!/_{\sum_{i=1}^{n} \frac{9\left(x_i^p - x_i^{mp}\right)^2}{x_i^{mp} D_i}\,/_{RT}} \tag{3}$$

where L is the average inter-particle spacing, f_p is the equilibrium volume fraction of the strengthening precipitates at the service temperature, r_0 is the critical precipitate nucleus size, γ is matrix-precipitate interfacial energy, ΔG_v is volume thermodynamic driving force for the precipitation. V_m^p is the molar volume of precipitate. K is the factor of coarsening rate and t is the exposure time at the high temperature. x is equilibrium interface mole fraction of the precipitation former elements on both matrix (m) and precipitate (p) sides. T is the service temperature and D is the corresponding diffusion coefficient. In the calculations the interfacial energy is arbitrarily set at a fixed value of 1 J m^{-2} irrespective of the precipitate size or type. This is a slight simplification but helps in illustrating the effect of precipitate coarsening. All thermodynamic parameter values including f_p, ΔG_v, x_i^p, x_i^{mp}, D_i, and V_m^p required during the calculations were calculated via Thermo-Calc using the TCFE6 and MOBFE1 databases. The equation shows that the highest strengthening factors are obtained for high volume fractions and small and constant precipitate sizes, that is, precipitates showing a very low coarsening rate. The computational details of the model and its application to MX precipitation strengthened creep resistant steel design can be found elsewhere.[25–27] In the

Table 2. The calculated microstructure of existing Cr-containing steels at 650 °C (in vol%, F indicates Ferrite and M indicates Martensite, with matrix to balance).

		Precipitates			
Grades	Matrix	$M_{23}C_6$	Laves	Z-phase	Others
P11/STB 22	F	2.84	-	-	
STBA23	F	2.82	-	-	
P22/STBA24	F	2.95	-	-	
STBA25	F	2.96	-	-	
P9/STBA26	F	3.00	-	-	
P91	M	1.99	-	0.60	
P92	M	1.40	1.10	0.50	
MARN	M	1.56	1.71	0.25	0.02NbC
NF12	M	2.00	1.63	0.64	$0.18M_2N$
SAVE12	M	1.85	1.99	0.37	0,07TaC
P122	M	2.20	1.35	0.67	$0.08M_2N$
15Cr3W3Co	F	2.00	3.10	0.59	$0.31M_2N$
15Cr6W3Co	F	1.00	6.70	0.50	

present calculations, the temperature and the creep time are fixed at 650 °C and 10^4 h, respectively.

With respect to solid solution strengthening, the solid solution strengthening factor was taken to be the weighted contribution of atomic concentration of solutes, which can be formulated as

$$\Delta\sigma_{ss} = a\sum_i S_i x_i^{mp} \quad (4)$$

where a is a temperature dependent scalar, and S_i is the (room temperature) solid solution strengthening coefficient which combines size misfit and modulus misfit effect. For the solid solution elements in this work, the strengthening coefficients at room temperature were determined from literature data on binary Fe–M systems and actual values are shown in **Table 3**.[28,29] Although in the reliable ranking of the alloy the actual value of a does not play a role, a value of $a = 0.25$ was used based on the calibration study in literature.[30]

The precipitation strengthening factors after 10^4 h at 650 °C due $M_{23}C_6$ and Laves phase contributions as well as the solid solution strengthening factors for the selected Cr containing steels are shown in **Figure 2**. It can be seen that the solid solution strengthening factor of all steels, marked by blue dots, fluctuates between 49 and 70 among all the grades. The much larger differences in creep strength shown in Figure 1 are mainly due to the difference in the contributions of precipitation strengthening. The black and red bars in Figure 2 shows that no great difference in the strengthening effect of $M_{23}C_6$ carbides can be found among the heat resistant steels, while the Laves phase

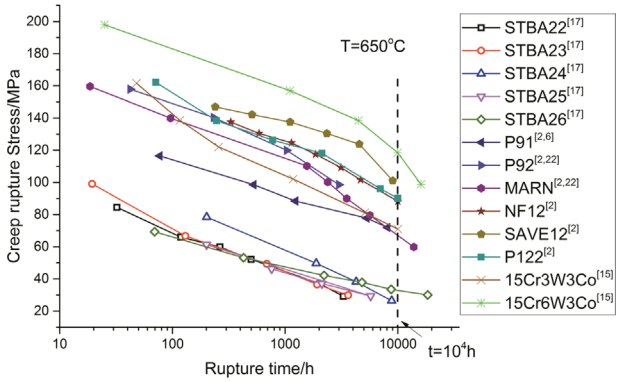

Figure 1. Stress-rupture data for heat resistant steels at 650 °C.

makes significantly different contributions to the creep strengthening. The sum of the precipitation strengthening factors matches the creep properties in Figure 1 with a reasonable sequence, which shows that 15Cr6W3Co performs best, followed by SAVE12 and NF12 alloys. The reason why only $M_{23}C_6$ and Laves phase are considered as strengthening phases in this calculation and the MX carbonitrides are ignored is due to the selected service time ($t = 10^4$ h) which in high Cr steels (Cr% $\geq$ 12) is sufficiently long for completion of the *Z*-phase formation depleting the MX carbonitrides population.[12] The coarse *Z*-phase precipitates do not contribute to the creep strength (i.e., at best do not introduce premature cracking) and are therefore also left out in the summation of strengthening factors. It should be mentioned that for the 9–11%Cr creep resistant steels the formation of *Z*-phase will not be finished completely in 10^4 h as a result of the lower thermodynamic driving force at lower Cr concentrations.[12] The result indicates that the calculated precipitation strengthening factors for P91, P92, NF12, and SAVE12 steels are underestimates since the contribution from retained MX carbonitrides is ignored.

In **Figure 3**, the experimental creep rupture stresses at 10^4 h obtained from the curves in Figure 1 are compared with the calculated precipitation strengthening factors from Figure 2. All data are within a linear scatter band as indicated by the two parallel dotted lines. As mentioned previously, the pre-set time 10^4 h is not sufficient long for complete *Z*-phase transformation in relative low-Cr (Cr% < 12) steels. As a result, the precipitation strengthening factors of P91, P92, NF12, and SAVE12 steels are underestimates due to effects of retained MX not being taking into account in the calculations. This is corresponding to the data points for P91, P92, NF12, and SAVE12 steels on the lower limit of the parallel dotted line. This suggest that a better linear relationship can be expected if the as yet non-quantifiable contributions of MX and *Z*-phase precipitates were taken into account. Nevertheless, by employing the current precipitation strengthening factor as the creep strength indicator and taking

Table 3. Strengthening coefficient for alloying elements at room temperature (MPa per at%).

Element	C	N	Si	Ni	Ti	Mn	Mo	W	Al	Cr	Co	V
S_i	1103.45	1103.45	25.80	19.20	17.90	16.90	15.90	31.8	9.00	2.60	2.10	2.00

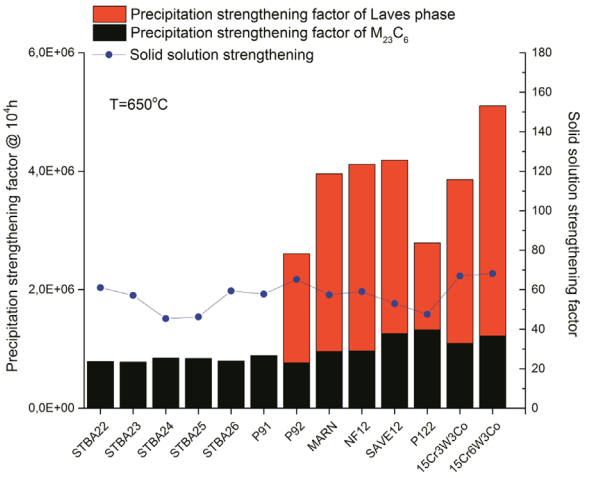

Figure 2. The calculated precipitation strengthening factor of $M_{23}C_6$ and Laves phase in existing Cr containing steels, at the temperature of 650 °C and service time of 10^4 h; and the calculated solid solution strengthening factor of existing Cr containing steels.

the contributions of solid solution strengthening as more or less constant, the model predicts the relative ranking of the selected commercial and pre-commercial steel grades rather well.

2.3. The Microstructural Changes as a Result of *Z*-Phase Formation

The formation of *Z*-phase and its consequence for so-called premature failure has been mentioned repeatedly in the literature when the experimental creep data and the corresponding changes in the microstructure were analyzed and correlated. To have a better understanding of the effect of *Z*-phase formation on the precipitate population, the thermodynamically calculated precipitate volume fractions in our selected heat resistant steelsare plotted in **Figure 4** with either the *Z*-phase computationally suppressed or allowed. The results show that for the alloys P91, MARN, SAVE12, and 15Cr6W3Co, the *Z*-phase

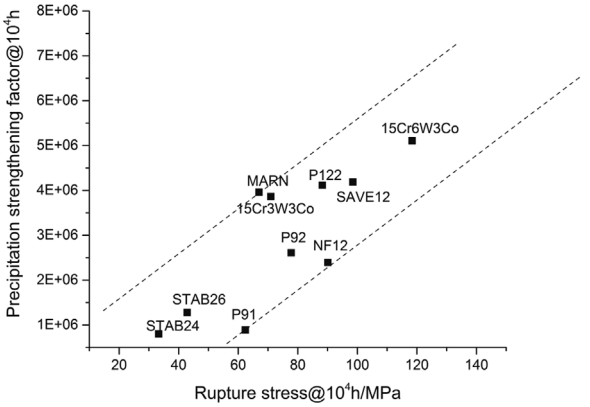

Figure 3. The calculated precipitation strengthening factor versus the experimental creep rupture for selected steels, both for exposure to 650 °C for 10^4 h.

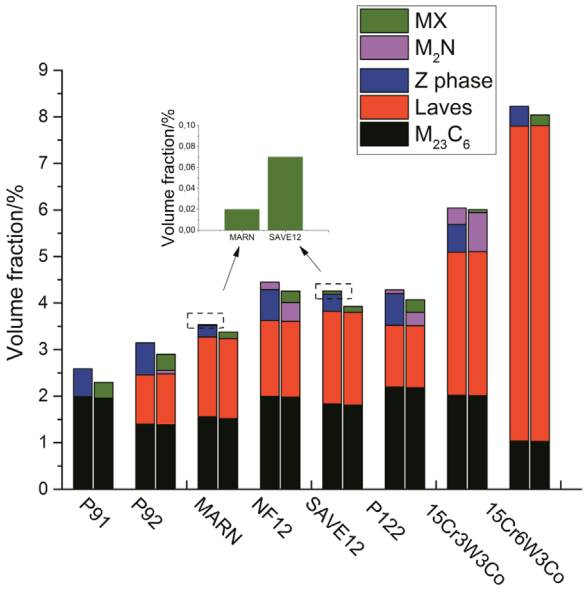

Figure 4. The calculated equilibrium precipitate populations (columns on left) and the precipitate populations with *Z*-phase being computationally suppressed (columns on right) for heat resistant steels.

develops solely at the expense of the strengthening MX particles. For the P92, NF12, P122, and 15Cr3W3Co alloys, the *Z*-phase not only originates from MX carbonitrides but also from M_2N particles. The predictions that M_2N nitrides partially transform into *Z*-phase particles agrees well with experimental observations.[31,32] However, no clear relationship between the maximum volume fraction of MX particles and the maximum amount of final *Z*-phase particles is found. To get this correlations clearer, a further investigation of the dislocation-pinning characteristics of consumed MX and the *Z*-phase particles formed would be required.

2.4. The Strength Loss Due to *Z*-Phase Formation

In the experimental creep curves shown in Figure 1, some steels show an accelerated degradation of the creep strength at long exposure times. To relate the accelerated strength loss to the *Z*-phase formation, the total precipitation strengthening factor is decomposed into its constituent terms using the results of the calculated microstructural changes shown in Figure 4. The black columns in **Figure 5** present the "stable strength" which is contributed by the equilibrium (i.e., surviving) Laves phase and $M_{23}C_6$ carbides, while the gray columns marks the contribution of the MX carbonitrides to the precipitation hardening before they are transformed into non-strength-contributing *Z*-phase particles. For the MARN and SAVE12 steels, only very small amounts of stable MX strengthening carbides are present. In the calculations, the (negative) contributions of both newly formed *Z*-phase and M_2N nitrides to the precipitation hardening factor are neglected, thus the sum of two represents the "ideal" precipitation hardening contribution. The results show that the precipitation related strength component of commercial grades P91 and P122 is almost halved after *Z*-phase formation, while

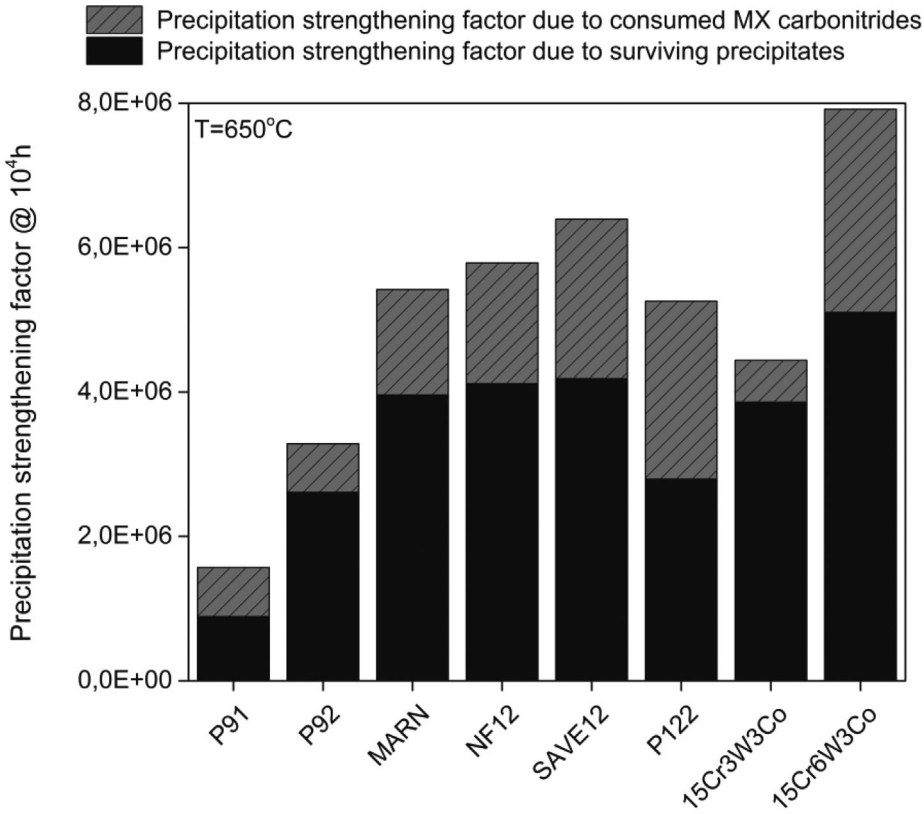

Figure 5. The calculated precipitation factor after 10^4 h due to the surviving precipitates ($M_{23}C_6$ + Laves phase) and the MX carbonitrides to be consumed in the *Z*-phase formation.

NF12, SAVE12, MARN, and 15Cr6W3Co steels only 1/3 of their precipitation strength is lost due to the disappearance of MX particles. The significant strength loss in precipitation strengthening factor as a result of the *Z*-phase formation encouraged us to conduct a more detailed analysis of the driving force for *Z*-phase formation.

2.5. The Driving Force for the *Z*-Phase Formation

Chromium has the most significant effect among all the alloying elements on the kinetics of *Z*-phase formation.[8] Experimental observations[12] show that in a 12%Cr steel the *Z*-phase precipitated 20 to 50 times faster than in 9%Cr steel, which is supported by a theoretical model indicating that an increase in Cr level strongly accelerates the *Z*-phase formation.[23] **Figure 6** shows the calculated driving force for *Z*-phase formation in exiting heat resistant steels, as well as the calculated upper and lower limit of *Z*-phase driving force with specification permitted C concentration differences as a function of Cr concentration in matrix as at 650 °C. From the middle black dash line in Figure 6, a clear linear relationship can be found between the calculated driving force of *Z*-phase in the selected steels and the Cr concentration in the matrix, which demonstrates that alloys with a high solid Cr concentration in solid solution are more prone to have a rapid *Z*-phase precipitation, while the transformation in low Cr steels should be more sluggish. Danielsen's simulation results[23] show that only Cr and C have a significant influence on the kinetics of *Z*-phase formation, while the effect of other *Z*-phase forming elements such as Nb, Mo, and V was found to be minor. The changes in *Z*-phase driving force as a function of the specification permitted C- content variations are shown in Figure 6 for the selected heat resistant steels. The blue spots mark the upper limit of *Z*-phase driving force for the minimum concentration of C concentration allowed in the steel specifications, while the red spots marks the *Z*-phase driving force for highest permitted C concentration. The blue and red dotted lines mark the variation range of the driving force in *Z*-phase transformation for the existing steels. The results indicate the possibility to reduce the driving force of *Z*-phase through tuning their element concentration. However, the adjustment in chemical concentration may cause complex synergies in thermodynamic as well as microstructural properties. The feasibility of element adjustment to lower the driving force for *Z*-phase formation will be discussed in the following paragraph.

2.6. Exploring the Option to Reduce the *Z*-Phase Formation at High Cr Levels

While on the one hand a high Chromium level is desirable because it leads to a better corrosion and oxidation resistance as

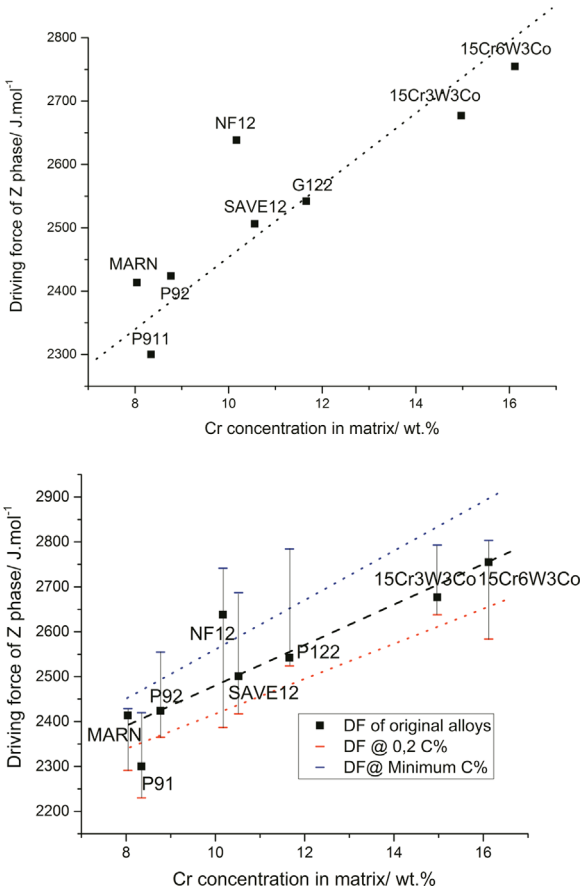

Figure 6. The calculated driving force for *Z*-phase formation in exiting heat resistant steels (in black dash line), as well as the calculated upper and lower limit of *Z*-phase driving force with specification permitted C concentration differences (in blue and red dot lines), as a function of Cr concentration in matrix as at 650 °C.

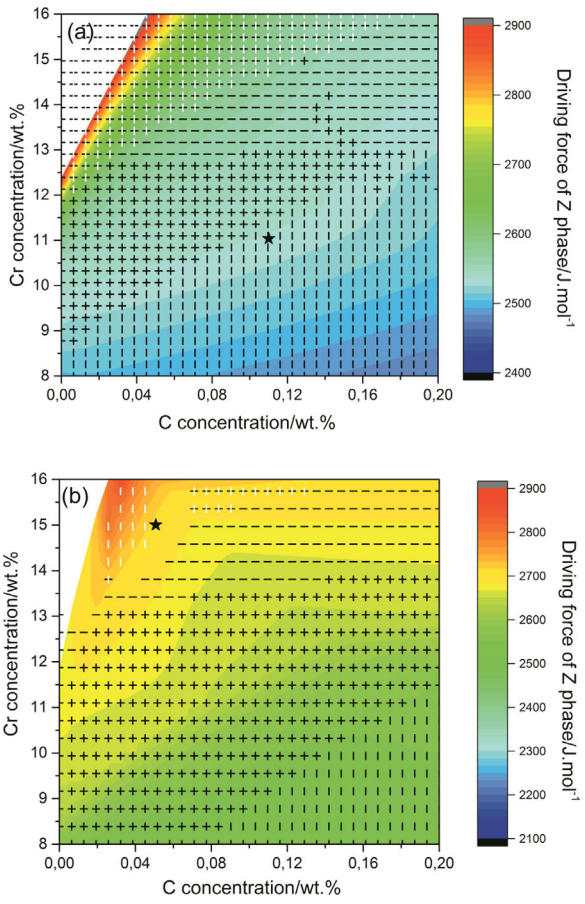

Figure 7. The binary isopleths of C–Cr for the calculated driving force of *Z*-phase in commercial grades a) P122 and b) 15Cr6W3Co steels. The black star symbols show the nominal concentration values for the P122 and 15Cr6W3Co alloys, respectively.

well as a higher initial strength, a high Cr level also leads to a high driving force for *Z*-phase formation and hence a more significant strength loss at long creep times. In **Figure 7**, the calculated driving force for *Z*-phase formation at 650 °C as a function of the two dominant alloying elements for *Z*-phase formation Cr and C[23] has been plotted, for two high Cr steels P122 and 15Cr6W3Co (see Table 1 for the concentration values for the other alloying elements) which showed the steepest drop in creep strength due to *Z*-phase formation. Using a graphical presentation mode first presented in reference[33] in each Figure, not only the driving force is presented via the background color contour but for each composition the thermodynamically predicted occurrence of other undesirable microstructural phenomena which would have a very negative effect on the creep performance, is indicated by different forms of shading. The black horizontal, black vertical, and white vertical slash patterns mark the domains where 1) the volume fraction of austenite at the homogenization temperature is less than 99% (i.e., δ ferrite or big primary carbides are present); 2) the Cr concentration in the matrix below 12% after formation of all equilibrium precipitates (i.e., the corrosion resistance would be poor); and 3) the volume fraction of undesirable intermetallic phase (excluding matrix, Laves phase, and $M_{23}C_6$ particles) at 650 °C is higher than 1%. The white regions close to the Cr-axis contain compositions where Thermo-Calc equilibrium calculation cannot be successfully performed. An unmarked areas would mark a composition region which would lead to the absence of undesirable microstructural phases and hence to optimal creep strength properties.

In Figure 7a, the background color contours show that *Z*-phase driving force rises with the increase of Cr concentration, while decreases as the C content increases, in agreement with the work by Danielsen. The Figure shows that (given the temperature of 650 °C and the other alloying element concentrations being at the level of those of the base alloy P122) there are no compositional domains which satisfy all constraints. The nominal P122 composition is located in the place where Cr concentration in solid solution in the matrix after formation of all precipitates is below the set level of 12%. In the middle area, the development of δ-ferrite consumes too much Cr in the matrix which reduces the volume fraction of austenite at the homogenisation temperature to unacceptably low levels, thereby, preventing the formation of a uniform martensitic microstructure. In the upper part of the Figure, high amounts of *Z*-phase

and σ phase are responsible for unattractive properties. The Figure clearly shows the P122 composition has some intrinsic deficiencies and a high tendency to form *Z*-phase but these characteristics cannot be resolved by adjustments in Cr or C level (nor by modest adjustments in any of the other alloying elements; results not shown but calculations performed).

In Figure 7b, a very narrow unmarked area can be found at the top left corner of the whole area, close to the nominal composition of 15Cr6W3Co steel, and this indicates that the composition of this steel grade is very well selected, but also that the steel has a high tendency to form *Z*-phases. This prediction is in excellent agreement with the experimental creep data as plotted in Figure 1, which shows the steel to have a the initial strength but a tendency to show accelerated creep strength loss at long testing times.

3. Conclusions

1) Heat resistant steels with different Cr levels have been employed. Their precipitation hardening effects and solid solution strengthening effects are calculated at 650 °C. The calculated creep properties has been compared with the experimental creep strength values and the results confirms that precipitation strengthening factor can reproduce the creep strength rather well.
2) The microstructural changes due to the long term exposure at 650 °C as a result of the *Z*-phase formation are analyzed using thermodynamics. The analysis indicates that accelerated creep strength loss is related to the consumption of the strengthening MX carbonitrides. At a service temperature of 650 °C, a high Cr level will unavoidably promote the formation of *Z*-phase.
3) By exploring the binary effect of two dominant alloying elements Cr and C on *Z*-phase formation, It was found not possible to propose compositional adjustments which lead to a combination of a high Cr level (12–15%Cr) and a reduced tendency to form *Z*-phase precipitates, while meeting all other requirements for a desirable starting microstructure.

Acknowledgements

This work was carried out with financial support from the Chinese Scholarship Council (CSC) as well as TU Delft internal funding. Prof. Wei XU acknowledges the financial support of the National Natural Science Foundation of China (No. 51722101 and No. 51574080).

Conflict of Interest

The authors declare no conflict of interest.

Keywords

chromium concentration, ferritic-martensitic steels steel, microstructure, *Z*-phase

Received: April 3, 2018
Revised: June 4, 2018
Published online: June 27, 2018

[1] F. Masuyama, *ISIJ Int*. **2001**, *41*, 612.
[2] F. Abe, T.-U. Kern, R. Viswanathan, *Creep-Resistant Steels*, Elsevier, Cambridge, England **2008**.
[3] F. Abe, *Mater. Sci. Eng. A* **2001**, *319*, 770.
[4] A. Mandal, T. K. Bandyopadhyay, *Steel Res. Int*. **2017**, *88*, 1600317.
[5] W. Yan, W. Wang, Y. Shan, K. Yang, *Front. Mater. Sci*. **2013**, *7*, 1.
[6] V. Sklenička, K. Kuchařová, M. Svoboda, L. Kloc, J. Buršk, A. Kroupa, *Mater. Charact*. **2003**, *51*, 35.
[7] K. Maruyama, K. Sawada, J.-I. Koike, *ISIJ Int*. **2001**, *41*, 641.
[8] H. K. Danielsen, J. Hald, *Energy Mater.* **2006**, *1*, 49.
[9] H. K. Danielsen, J. Hald, *Mater. Sci. Eng. A* **2009**, *505*, 169.
[10] J. Hald, *Trans. Indian Inst. Met*. **2016**, *69*, 183.
[11] A. Strang, V. Vodarek, *Mater. Sci. Technol. —Lond*. **1996**, *12*, 552.
[12] H. K. Danielsen, P. E. Di Nunzio, J. Hald, *Metall. Mater. Trans. A* **2013**, *44*, 2445.
[13] J. Lopez Barrilao, B. Kuhn, E. Wessel, M. Talík, *Mater. Sci. Technol. —Lond*. **2017**, *33*, 1056.
[14] K. Kimura, H. Kushima, E. Baba, T. Shimizu, Y. Asai, F. Abe, K. Yagi, *Tetsu-to-Hagané* **2000**, *86*, 542.
[15] K. Kimura, K. Seki, Y. Toda, F. Abe, *ISIJ Int*. **2001**, *41*, S121.
[16] W. Quadakkers, J. Zurek, *Shreir's Corros*. **2010**, *1*, 407.
[17] T.-U. Kern, G. Merckling, K. Yagi, In *Creep Properties of Heat Resistant Steels and Superalloys*, Springer, Berlin, Heidelberg **2000**, p. 1.
[18] F. Abe, M. Tabuchi, S. Tsukamoto, H. Kutsumi, In ASME 2014 Symposium on Elevated Temperature Application of Materials for Fossil, Nuclear, and Petrochemical Industries, (American Society of Mechanical Engineers: Seattle, Washington, USA **2014**), p. 44.
[19] M. Igarashi, Y. Sawaragi, In *International Conference on Power Engineering-97 (ICOPE-97)*, *Tokyo, Japan*, **1997**, p. 107.
[20] J. Svoboda, *ASM Handbook* **1988**, *15*, 715.
[21] F. Abe, *Int. J. Mater. Res*. **2008**, *99*, 387.
[22] M. Hättestrand, H.-O. Andrén, *Mater. Sci. Eng. A* **1999**, *270*, 33.
[23] H. K. Danielsen, J. Hald, *Calphad* **2007**, *31*, 505.
[24] F. Abe, In *Advances in Science and Technology*, Trans Tech Publ., Switzerland **2010**, p. 12.
[25] Q. Lu, W. Xu, S. van der Zwaag, *Philos. Mag*. **2013**, *93*, 3391.
[26] Q. Lu, W. Xu, S. van der Zwaag, *Acta Mater.* **2014**, *77*, 310.
[27] Q. Lu, W. Xu, S. van der Zwaag, *Comp. Mater. Sci*. **2014**, *84*, 198.
[28] F. B. Pickering, *Physical Metallurgy and the Design of Steels*, Applied Science Publishers, London **1978**.
[29] W. C. Leslie, *Metall. Mater. Trans. B* **1972**, *3*, 5.
[30] Q. Lu, W. Xu, S. van der Zwaag, *Comp. Mater. Sci*. **2014**, *84*, 198.
[31] K.-H. Lee, J.-Y. Suh, S.-M. Hong, J.-Y. Huh, W.-S. Jung, *Mater. Charact*. **2015**, *106*, 266.
[32] L. Cipolla, H. K. Danielsen, D. Venditti, P. E. Di Nunzio, J. Hald, M. A. J. Somers, *Acta Mater.* **2010**, *58*, 669.
[33] W. Xu, P. R. D. Del Castillo, S. van der Zwaag, *Int. J. Mod. Phys. B* **2009**, *23*, 1060.

